Progress In Electromagnetics Research, PIER 25, 1–22, 2000

TVFEM ANALYSIS OF PERIODIC STRUCTURES FOR RADIATION AND SCATTERING

Y. Zhu and R. Lee

ElectroScience Laboratory
Department of Electrical Engineering
The Ohio State University
1320 Kinnear Road
Columbus, OH 43212, USA

1. INTRODUCTION

There are many applications in electromagnetics involving periodic structures, such as a periodically loaded waveguide, a frequency selective surface (FSS), and a phased array antenna. To design devices with specific electromagnetic scattering or radiation characteristics in terms of their periodicity, geometrical layout, and composite media, a general electromagnetic modeling and characterization method, which is accurate and efficient, is needed. The finite element method (FEM) is very suitable for the analysis of periodic structures, because after the appropriate imposition of the periodic boundary condition, the computational domain for an infinite periodic array can be reduced to a single unit cell which is usually in the order of a wavelength. Furthermore, the FEM is a general and powerful electromagnetic modeling tool. It

can easily deal with problems of arbitrary complexity in both geometry and material composition; it generates a sparse system matrix which is efficient in terms of both the memory storage and the CPU time. In this paper, the analysis of periodic structures will be addressed using the FEM.

Depending on the different types of basis functions, the FEM used for solving the electromagnetic (EM) problems can be divided into two major categories: nodal FEM and tangentially continuous vector FEM (TVFEM). TVFEM uses vector basis functions which impose the tangential continuity, but allow the normal discontinuity on the interface between two adjacent elements. The property of TVFEM has many advantages over the traditional nodal FEM, including easy imposition of boundary and interface conditions, absence of spurious modes, and the ability to model PEC singularity. Therefore, TVFEM has been widely used in the FEM community in recent years. This paper mainly focuses on TVFEM to analyze periodic structures.

Several attempts have been made to study periodic structure by combining the FEM with other techniques. In [1, 2], a two-dimensional hybrid finite element/boundary element approaches addressing the infinite grating problems has been reported. The three-dimensional finite-element /boundary integral combination was presented in [3–6]. In this approach, the field within the periodic cell is described by finite elements, the field outside the periodic cell is expressed by the boundary integral equation with the periodic Green's function or by Floquent harmonic expansion. The two fields are coupled at the interface using the continuity of tangential fields. This approach is complex in its implementation, and it introduces a full sub-matrix into the sparse system matrix, which is expensive in terms of both computation time and memory requirement.

In this paper, the anisotropic perfectly matched layer (PML) [7] is used to truncate the computational domain. The PML is placed at a certain distance above/below the array to absorb the outgoing plane waves. Compared with the boundary integral technique, the implementation of the PML can be easily combined into the FEM code, and the system matrix still possesses its sparsity property. Also, in this paper, we offers a detailed formulation for the imposition of the periodic boundary condition in TVFEM. The implementation makes use of the basic property of TVFEM. Both $H_0(curl)$ and $H_1(curl)$ space are discussed. Following the formulation, we show numerical

examples for a waveguide array as well as plane wave scattering by a dielectric slab, a metal mesh, and a metal patch array to assess the validity and accuracy of the method.

2. GENERAL FORMULATION

Consider a single unit cell in an infinite periodic array, shown in Figure 1. The array can be excited by an external source such as a plane wave denoted by $\vec{E}^{inc}$ for scattering problems. It can also be excited by an impressed electric and magnetic current, $\vec{J}_i$ and $\vec{M}_i$ within the unit cell representing feeding structures for antennas such as a waveguide or coaxial-line aperture on a PEC ground plane. The anisotropic PML is placed at a certain distance above and below the unit cell to absorb the outgoing wave $\vec{E}^{out}$, which in general can be a superposition of the scattered field due to $\vec{E}^{inc}$ and the radiation field from $\vec{J}_i$ and $\vec{M}_i$. The outer surfaces of the PML is terminated with a perfect electric conductors (PEC). The total computational domain Ω is bounded by the PEC and four side walls.

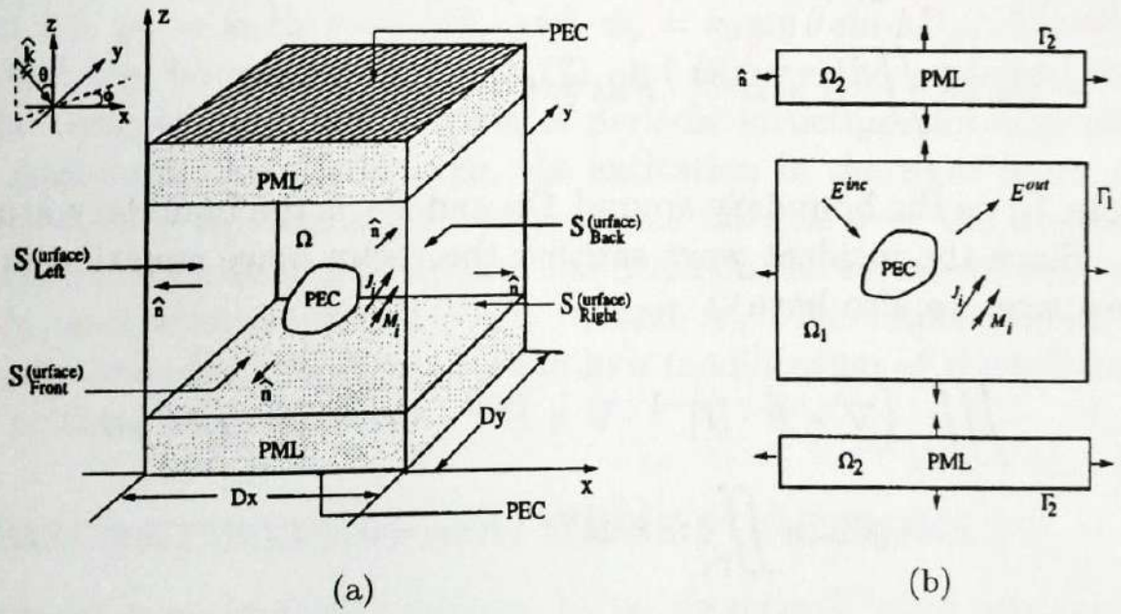

(a) (b)

Figure 1. (a) A unit cell in an infinite array, (b) Front view of the cell.

In the non-PML region Ω_1 excluding any PEC region, the total electric field $\vec{E}$ satisfies the vector wave equation

$$\nabla \times [\mu_r]^{-1} \nabla \times \vec{E} - k_0^2 [\epsilon_r] \vec{E} = -jk_0 Z_0 \vec{J}_i - \nabla \times \left([\mu]^{-1} \vec{M}_i \right) , \quad (1)$$

and the essential boundary condition $\hat{n} \times \vec{E} = 0$ on the surface of the PEC in Ω_1.

In the PML region Ω_2, the outgoing electric field satisfies the vector wave equation:

$$\nabla \times [\mu_r]^{-1} \nabla \times \vec{E}^{out} - k_0^2 [\epsilon_r] \vec{E}^{out} = 0, \tag{2}$$

and the essential boundary condition $\hat{n} \times \vec{E}^{out} = 0$ on the surface of the PEC at the back of the two PML regions.

By multiplying the equation (1) and (2) with an arbitrary weighting function $\vec{F}$, and integrating over their computational domains, we get two weak form equations for (1) and (2), respectively:

$$\begin{aligned} &\iiint_{\Omega_1} \left(\nabla \times \vec{F} \cdot [\mu_r]^{-1} \cdot \nabla \times \vec{E} - k_0^2 F \cdot [\epsilon_r] \cdot \vec{E} \right) dv - jk_0 Z_0 \iint_{\Gamma_1} \hat{n} \times \vec{H} \cdot \vec{F} ds \\ &= - \iiint_{\Omega_1} \vec{F} \cdot \left[jk_0 Z_0 \vec{J}_i + \nabla \times \left([\mu]^{-1} \vec{M}_i \right) \right] dv, \end{aligned} \tag{3}$$

$$\begin{aligned} &\iiint_{\Omega_2} \left(\nabla \times \vec{F} \cdot [\mu_r]^{-1} \cdot \nabla \times \vec{E}^{out} - k_0^2 F \cdot [\epsilon_r] \cdot \vec{E}^{out} \right) dv \\ &- jk_0 Z_0 \iint_{\Gamma_2} \hat{n} \times \vec{H}^{out} \cdot \vec{F} ds = 0, \end{aligned} \tag{4}$$

where Γ_1 is the boundary around Ω_1 and Γ_2 is the boundary around Ω_2. Since the incident wave satisfies the vector wave equation in the free space, we also have

$$\begin{aligned} &\iiint_{\Omega_1} \left(\nabla \times \vec{F} \cdot [I]^{-1} \cdot \nabla \times \vec{E}^{inc} - k_0^2 \vec{F} \cdot [I] \cdot \vec{E}^{inc} \right) dv \\ &- jk_0 Z_0 \iint_{\Gamma_1} \hat{n} \times \vec{H}^{inc} \cdot \vec{F} ds = 0. \end{aligned} \tag{5}$$

Because we want to get the outgoing field formulation, we split $\vec{E} = \vec{E}^{inc} + \vec{E}^{out}$ and $\vec{H} = \vec{H}^{inc} + \vec{H}^{out}$ in (3), delete the surface integral about $\hat{n} \times \vec{H}^{inc} \cdot \vec{F}$ on Γ_1 using (5), and add it with (4) to get

$$\begin{aligned} &\iiint_{\Omega} \left(\nabla \times \vec{F} \cdot [\mu_r]^{-1} \cdot \nabla \times \vec{E}^{out} - k_0^2 \vec{F} \cdot [\epsilon_r] \cdot \vec{E}^{out} \right) dv \\ &- jk_0 Z_0 \iint_{S_L + S_R + S_F + S_B} \hat{n} \times \vec{H}^{out} \cdot \vec{F} ds \end{aligned}$$

$$= -\iiint_{\Omega_1} \left(\nabla \times \vec{F} \cdot ([\mu_r]^{-1} - [I]) \cdot \nabla \times \vec{E}^{inc} - k_0^2 \vec{F} \cdot ([\epsilon_r] - [I]) \cdot \vec{E}^{inc} \right) dv$$
$$- \iiint_{\Omega_1} \vec{F} \cdot \left[jk_0 Z_0 \vec{J}_i + \nabla \times \left([\mu]^{-1} \vec{M}_i \right) \right] dv \,, \tag{6}$$

where the essential boundary condition is

$$\begin{aligned} \hat{n} \times \vec{E}^{out} &= -\hat{n} \times \vec{E}^{inc} \qquad \text{on the surface of PEC in } \Omega_1 \\ \hat{n} \times \vec{E}^{out} &= 0 \qquad \text{on the surface of PEC backing the PML,} \end{aligned} \tag{7}$$

The periodic boundary condition on the four side walls is

$$\begin{aligned} \hat{n} \times \vec{E}^{out}_{Right} &= -\hat{n} \times \vec{E}^{out}_{Left} e^{-j\psi_x} \\ \hat{n} \times \vec{H}^{out}_{Right} &= -\hat{n} \times \vec{H}^{out}_{Left} e^{-j\psi_x} \\ \hat{n} \times \vec{E}^{out}_{Front} &= -\hat{n} \times \vec{E}^{out}_{Back} e^{-j\psi_y} \\ \hat{n} \times \vec{H}^{out}_{Front} &= -\hat{n} \times \vec{H}^{out}_{Back} e^{-j\psi_y} \end{aligned} \tag{8}$$

Here, ψ_x and ψ_y are phase shift between the opposing walls along x and y direction due to the source excitation. These phase shifts are given by $\psi_x = k_0 \sin\theta \cos\phi D_x$ and $\psi_y = k_0 \sin\theta \sin\phi D_y$. Equation (6) and the boundary condition (7) and (8) are the preferred form of the outgoing field formulation of periodic structures for scattering and radiation. As can be seen, the excitation in the right hand side of the system equations (6) is the volume integral over the dielectric scatterers, the essential boundary condition on the surface of the PEC in Ω_1, and volume integral about $\vec{J}_i$ and $\vec{M}_i$. The imposition of the periodic boundary condition results in a modification of the left hand side of the system equation.

3. DISCRETIZATION AND BASIS FUNCTIONS

The total computational domain Ω is discretized using tetrahedra. Each node in the mesh is given a node number i; each edge is denoted by an ordered node pair $\{i, j\}$; each face is by an ordered node triple $\{i, j, k\}$. The electric field inside the domain Ω and on the boundary surface as well as the magnetic field on the boundary surface are approximated by the following expansion

$$\vec{E} = \sum_{n=0}^{N} \vec{\psi}_n e_n = \vec{\psi}^T \cdot \mathbf{e}, \qquad \vec{H} = \sum_{n=0}^{M} \vec{\psi}_n h_n = \vec{\psi}^T \cdot \mathbf{h}_b, \tag{9}$$

where $\vec{\psi}_n$ is the vector basis function, e_n and h_n are the scalar expansion coefficient, N is number of total unknowns, and M is the number of unknowns on the boundary. Two kinds of basis function spaces, i.e., $H_0(curl)$ and $H_1(curl)$, are commonly used in TVFEM [8, 9].

For $H_0(curl)$ space, the vector basis function is associated with the edges of tetrahedron.

$$\vec{v}_{ij} = \lambda_i \nabla \lambda_j - \lambda_i \nabla \lambda_i, \qquad \text{for edge } \{i, j\} \tag{10}$$

For $H_1(curl)$ space, the vector basis functions in a tetrahedron can be divided into two groups:

edge basis functions

$$\vec{u}_{ij} = \lambda_i \nabla \lambda_i \quad \text{and} \quad \vec{u}_{ji} = \lambda_j \nabla \lambda_i \quad \text{for edge } \{i, j\}; \tag{11}$$

face basis functions

$$\vec{w}_0 = 4\lambda_i \left(\lambda_j \nabla \lambda_k - \lambda_k \nabla \lambda_j\right) \quad \text{and} \quad \vec{w}_1 = 4\lambda_j \left(\lambda_k \nabla \lambda_i - \lambda_i \nabla \lambda_k\right) \quad \text{for face } \{i, j, k\}. \tag{12}$$

The basic property of TVFEM spaces is that the basis functions guarantee the tangential component of the field across the interface between two adjacent elements is continuous, while the normal component is allowed to be discontinuous. The periodic boundary condition (8) specifies that the electric and magnetic fields on a given side wall are the same as those on the opposing side wall, except for a possible constant phase shift. Therefore, in order to impose the periodic boundary condition (8), one only needs to impose a phase-shift relationship between unknown coefficients on the opposing side walls.

For ease of implementation, the surface meshes on the opposing walls have to be identical, but the corresponding tetrahedra do not necessarily have to be identical. Meanwhile, the node order for two image edges or faces on opposing walls should map to each other, which guarantees the basis functions for the two image edges or faces are related because the basis function is determined by the order of nodes. Another requirement is the global unknown coefficient vector e

and $\mathbf{h}_b$ should be arranged such that,

$$\mathbf{e}\begin{pmatrix}\mathbf{e}_i\\ \mathbf{e}_b\end{pmatrix} \quad \mathbf{h}_b = \begin{pmatrix}\mathbf{h}_{L(eft)}\\ \mathbf{h}_{L-F}\\ \mathbf{h}_{L-B}\\ \mathbf{h}_{F(ront)}\\ \mathbf{h}_{R(ight)}\\ \mathbf{h}_{R-F}\\ \mathbf{h}_{R-B}\\ \mathbf{h}_{B(ack)}\end{pmatrix}, \qquad \text{where } \mathbf{e}_b = \begin{pmatrix}\mathbf{e}_{L(eft)}\\ \mathbf{e}_{L-F}\\ \mathbf{e}_{L-B}\\ \mathbf{e}_{F(ront)}\\ \mathbf{e}_{R(ight)}\\ \mathbf{e}_{R-F}\\ \mathbf{e}_{R-B}\\ \mathbf{e}_{B(ack)}\end{pmatrix}. \tag{13}$$

Here, $\mathbf{e}_i$ is the unknown vector whose elements are inside Ω; $\mathbf{e}_L$ and $\mathbf{h}_L$, $\mathbf{e}_F$ and $\mathbf{h}_F$, $\mathbf{e}_R$ and $\mathbf{h}_R$, $\mathbf{e}_B$ and $\mathbf{h}_B$ are the unknown vectors whose elements are on the left, front, right and back wall, respectively; $\mathbf{e}_{L-F}$ and $\mathbf{h}_{L-F}$, $\mathbf{e}_{L-B}$ and $\mathbf{h}_{L-B}$, $\mathbf{e}_{R-F}$ and $\mathbf{h}_{R-F}$, $\mathbf{e}_{R-B}$ and $\mathbf{h}_{R-B}$ are the unknown vectors whose elements are on the left-front, left-back, right-front, and right-back edge, respectively.

Substituting the expansion (9) into the LHS of the equation (6), and applying Galerkin's formulation, i.e., let $\vec{F} = \vec{\psi}$, we get the system matrix

$$\begin{aligned}
&\iiint_\Omega \left(\nabla \times \vec{F} \cdot [\mu_r]^{-1} \cdot \nabla \times \vec{E} - k_0^2 \vec{F} \cdot [\epsilon_r] \cdot \vec{E}\right) dv \\
&\quad - jk_0 Z_0 \iint_{S_L+S_R+S_F+S_B} \hat{n} \times \vec{H} \cdot \vec{F} ds \\
&= [S]_{N\times N} \cdot \mathbf{e} - jk_0 Z_0 [U]_{N\times M} \cdot \mathbf{h}_b \\
&= \begin{pmatrix} S_{i,i} & S_{i,b} \\ S_{b,i} & S_{b,b}\end{pmatrix} \cdot \begin{pmatrix}\mathbf{e}_i \\ \mathbf{e}_b\end{pmatrix} - jk_0 Z_0 \begin{pmatrix}0 \\ P\end{pmatrix} \cdot \mathbf{h}_b,
\end{aligned} \tag{14}$$

where

$$\begin{aligned}
[S]_{i,j} &= \iiint_\Omega \left(\nabla \times \vec{\psi}_i \cdot [\mu_r]^{-1} \cdot \nabla \times \vec{\psi}_j - k_0^2 \vec{\psi}_i \cdot [\epsilon_r] \cdot \vec{\psi}_j\right) dv \\
[U]_{i,j} &= \iint_s \hat{n} \times \vec{\psi}_j \cdot \vec{\psi}_i ds.
\end{aligned} \tag{15}$$

In the system matrix (14), the number of equations is N, while the number of unknowns is $N + M$. Therefore, the periodic boundary condition is needed here to solve the system matrix.

4. IMPOSITION OF THE PERIODIC BOUNDARY CONDITION

The discussion about the imposition of periodic boundary condition focuses on the system matrix (14). However, before we proceed with the discussion, it is necessary to obtain the structure of the matrix P.

$$[P]_{i,j} = \int_s \hat{n} \times \vec{\psi}_j \cdot \vec{\psi}_i ds \tag{16}$$

From the basic property of TVFEM spaces, we can obtain two properties about the integral (16).

a: If the unknown coefficients associated with $\vec{\psi}_i$ and $\vec{\psi}_j$ are not both in the plane s, $\iint_s \hat{n} \times \vec{\psi}_j \cdot \vec{\psi}_i ds = 0$ as shown in Figure 2.a

b: The two integrals on two opposing walls have the relationship: $\iint_s \hat{n} \times \vec{\psi}_j \cdot \vec{\psi}_i ds = -\iint_{s'} \hat{n} \times \vec{\psi}_{j'} \cdot \vec{\psi}_{i'} ds$ as shown in Figure 2.b

Making use of the two properties about $[P]_{i,j}$, we obtain the structure of matrix P,

$$P \cdot \mathbf{h}_b = \begin{pmatrix} A & X_1 & X_2 & 0 & 0 & 0 & 0 & 0 \\ -X_1^T & Y_1+Y_2 & 0 & -X_3^T & 0 & 0 & 0 & 0 \\ -X_2^T & 0 & -Y_2+Y_3 & 0 & 0 & 0 & 0 & X_3^T \\ 0 & X_3 & 0 & B & 0 & X_4 & 0 & 0 \\ 0 & 0 & 0 & 0 & -A & -X_1 & -X_2 & 0 \\ 0 & 0 & 0 & -X_4^T & X_1^T & -Y_1-Y_4 & 0 & 0 \\ 0 & 0 & 0 & 0 & X_2^T & 0 & Y_4-Y_3 & X_4^T \\ 0 & 0 & -X_3 & 0 & 0 & 0 & -X_4 & -B \end{pmatrix} \cdot \begin{pmatrix} \mathbf{h}_L \\ \mathbf{h}_{L-F} \\ \mathbf{h}_{L-B} \\ \mathbf{h}_F \\ \mathbf{h}_R \\ \mathbf{h}_{R-F} \\ \mathbf{h}_{R-B} \\ \mathbf{h}_B \end{pmatrix} \tag{17}$$

In the TVFEM modeling, the periodic boundary condition (8) turns out to be the relationship between the unknown coefficients on the opposing walls.

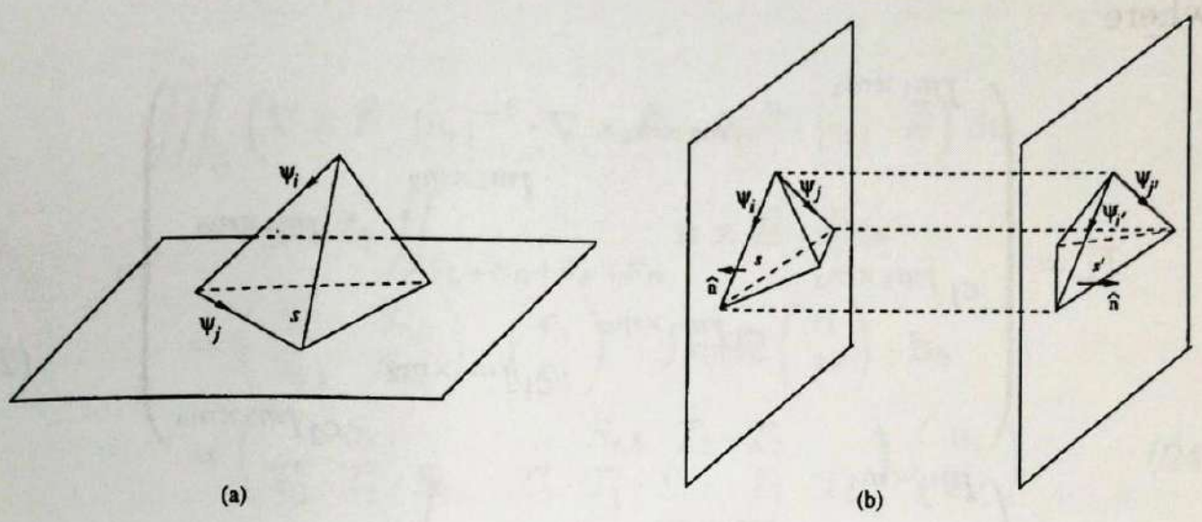

Figure 2. Two properties about the integral, $[P]_{i,j} = \iint_s \hat{n} \times \vec{\psi}_j \cdot \vec{\psi}_i ds$.

$$\begin{pmatrix} \mathbf{e}_R \\ \mathbf{e}_{R-F} \\ \mathbf{e}_{R-B} \\ \mathbf{e}_B \end{pmatrix} = \begin{pmatrix} c_1 I^{m_1 \times m_1} & & & \\ & c_1 I^{m_2 \times m_2} & & \\ & & c_1 I^{m_2 \times m_2} & \\ & & & c_2 I^{m_3 \times m_3} \end{pmatrix} \cdot \begin{pmatrix} \mathbf{e}_L \\ \mathbf{e}_{L-F} \\ \mathbf{e}_{L-B} \\ \mathbf{e}_F \end{pmatrix},$$

$$\mathbf{e}_{L-B} = \left(c_2 I^{m_2 \times m_2}\right) \mathbf{e}_{L-F}, \tag{18}$$

$$\begin{pmatrix} \mathbf{h}_R \\ \mathbf{h}_{R-F} \\ \mathbf{h}_{R-B} \\ \mathbf{h}_B \end{pmatrix} = \begin{pmatrix} c_1 I^{m_1 \times m_1} & & & \\ & c_1 I^{m_2 \times m_2} & & \\ & & c_1 I^{m_2 \times m_2} & \\ & & & c_2 I^{m_3 \times m_3} \end{pmatrix} \cdot \begin{pmatrix} \mathbf{h}_L \\ \mathbf{h}_{L-F} \\ \mathbf{h}_{L-B} \\ \mathbf{h}_F \end{pmatrix},$$

$$\mathbf{h}_{L-B} = \left(c_2 I^{m_2 \times m_2}\right) \mathbf{h}_{L-F}, \tag{19}$$

where $c_1 = e^{-j\psi_x}$, $c_2 = e^{-j\psi_y}$; m_1 is the number of unknowns in the left or right surface; m_2 is the number of unknowns on an edge; m_3 is the number of unknowns in the front or back surface. From the surface coefficient relationship (18) and (19), we obtain

$$\mathbf{e}_b = T_1 \cdot T_2 \cdot \begin{pmatrix} \mathbf{e}_L \\ \mathbf{e}_{L-F} \\ \mathbf{e}_F \end{pmatrix} \qquad \mathbf{h}_b = T_1 \cdot T_2 \cdot \begin{pmatrix} \mathbf{h}_L \\ \mathbf{h}_{L-F} \\ \mathbf{h}_F \end{pmatrix} \tag{20}$$

where

$$T_1 = \begin{pmatrix} I^{m_1\times m_1} & & & & \\ & I^{m_2\times m_2} & & & \\ & & I^{m_2\times m_2} & & \\ & & & I^{m_3\times m_3} & \\ c_1 I^{m_1\times m_1} & & & & \\ & c_1 I^{m_2\times m_2} & & & \\ & & c_1 I^{m_2\times m_2} & & \\ & & & c_2 I^{m_3\times m_3} & \end{pmatrix}, \tag{21}$$

$$T_2 = \begin{pmatrix} I^{m_1\times m_1} & & \\ & I^{m_2\times m_2} & \\ & c_2 I^{m_2\times m_2} & \\ & & I^{m_3\times m_3} \end{pmatrix}.$$

From the structure of the matrix P, we could find the identity

$$T_2' \cdot T_1' \cdot P \cdot T_1 \cdot T_2 = 0, \tag{22}$$

where

$$T_1' = \begin{pmatrix} I^{m_1\times m_1} & & & & \\ & I^{m_2\times m_2} & & & \\ & & I^{m_2\times m_2} & & \\ & & & I^{m_3\times m_3} & \\ \frac{1}{c_1} I^{m_1\times m_1} & & & & \\ & \frac{1}{c_1} I^{m_2\times m_2} & & & \\ & & \frac{1}{c_1} I^{m_2\times m_2} & & \\ & & & \frac{1}{c_2} I^{m_3\times m_3} & \end{pmatrix},$$

and

$$T_2' = \begin{pmatrix} I^{m_1\times m_1} & & & \\ & I^{m_2\times m_2} & \frac{1}{c_2} I^{m_2\times m_2} & \\ & & & I^{m_3\times m_3} \end{pmatrix}. \tag{23}$$

Substituting (20) into the system matrix (14) and using the identity (22), we get the system matrix for periodic structures

$$\iiint_{\Omega} \left(\nabla \times \vec{F} \cdot [\mu_r]^{-1} \cdot \nabla \times \vec{E} - k_0^2 \vec{F} \cdot [\epsilon_r] \cdot \vec{E} \right) dv$$

$$- jk_0 Z_0 \iint_{S_L+S_R+S_F+S_B} \hat{n} \times \vec{H} \cdot \vec{F} ds$$

$$= \begin{pmatrix} S_{i,i} & S_{i,b} \\ S_{b,i} & S_{b,b} \end{pmatrix} \cdot \begin{pmatrix} \mathbf{e}_i \\ \mathbf{e}_b \end{pmatrix} - jk_0 Z_0 \begin{pmatrix} 0 \\ P \end{pmatrix} \cdot \mathbf{h}_b$$

$$= \begin{pmatrix} S_{i,i} & S_{i,b} \cdot T_1 \cdot T_2 \\ T_2' \cdot T_1' \cdot S_{b,i} & T_2' \cdot T_1' \cdot S_{b,b} \cdot T_1 \cdot T_2 \end{pmatrix} \begin{pmatrix} \mathbf{e}_i \\ \mathbf{e}_{b'} \end{pmatrix}, \qquad (24)$$

where $\mathbf{e}_{b'} = (\mathbf{e}_L^T, \ \mathbf{e}_{L-F}^T, \ \mathbf{e}_F^T)$. The imposition of the periodic boundary condition can be viewed mathematically as column manipulations (right multiplication with T_1 and T_2) and row manipulations (left multiplication with T_1' and T_2') of the system matrix to merge the coefficients on the opposing walls.

5. UPPER AND BOTTOM BOUNDARY TRUNCATION: PML

The upper and bottom boundary of the computational domain Ω are truncated by the anisotropic PML. The permeability and permittivity matrix of the PML [7, 10] are:

$$[\epsilon] = \epsilon_0 \Lambda, \quad [\mu] = \mu_0 \Lambda, \quad \text{and } \Lambda = \begin{bmatrix} \alpha - j\beta & & \\ & \alpha - j\beta & \\ & & \dfrac{1}{\alpha - j\beta} \end{bmatrix} \qquad (25)$$

The special property of the PML guarantees that when a plane wave propagates through an infinite interface between the free space and the PML, there is no reflection for any incidence angle and polarization. Meanwhile, the PML is lossy so that the plane wave decays while it propagates in the PML. As we know from the Floquent harmonic expansion [6], illuminating an infinite array with a monochromatic plane wave results in a scattered field that is composed of an infinite sets of plane waves (Floquent harmonics). A finite number of these waves propagate away from the array, the remaining waves attenuate along the normal direction of the array. Since the PML is capable of absorbing plane waves very well, we put the PML above/below the

array by a fraction of a wavelength to absorb the outgoing plane waves. Four parameters of the PML need to be determined, i.e., the height of the PML, the thickness of PML, and the values of α and β. For a PEC-backed PML, the reflection coefficient is

$$|R(\theta_i)| = e^{-2\beta k_0 t \cos\theta_i}, \quad \text{or } |R(\theta_i)| = -17.372\beta k_0 t \cos\theta_i (dB), \quad (26)$$

where θ_i is the incidence angle of the plane wave, t is the thickness of the PML. In our implementation, t is chosen to be $0.2\lambda_0$; β is chosen from (26) so that R has -40 dB attenuation. Theoretically, α has no effect on the absorption capability of the PML, it only affects the wavelength in the PML, usually we let $\alpha = \beta$ to provide a good compromise between the discretization error and the convergence speed [11]. The height of the PML is determined by the attenuation rate of the high order modes, its selection is a compromise between the number of unknowns and absorption performance of the PML. Our results were accurate when we placed the PML $0.3\lambda_0$ away from array.

6. NUMERICAL RESULTS

To validate the method, numerical results are generated for various geometries and compared to available solutions in the literature. A bi-conjugate gradient solver (BiCG) with diagonal preconditioning is used to solve the resulting matrix equations.

In the first example, an infinite array of open rectangular waveguides arranged in a rectangular grid is analyzed [12, 13]. Two cases are tested. The first is a thin-walled waveguide array, and second is a thick-walled waveguide array. Figures 3 and 4 show the geometry of the waveguide array and the magnitude of reflection coefficient R in terms of scan angle θ from 0° to 60° for the H plane scan in these two cases. For both cases, the PML is $0.23\lambda_0$ thick and placed $0.29\lambda_0$ above the ground plane. The average edge length is $0.057\lambda_0$. From the Floquent harmonic expansion, we know when $0 \le \theta \le \sin^{-1}(\lambda_0/D_x)$, only the $(0,0)$ mode propagates from the array. Where θ increases, the $(-1,0)$ mode decays more and more slowly along z direction. After $\theta > \sin^{-1}(\lambda_0/D_x)$, the $(-1,0)$ mode becomes a propagating mode. It propagates at the grazing angle, and then rises up. In this analysis, $\beta = 2.0$ for $\theta = 0°$-$20°$; $\beta = 2.5$ for $\theta = 25°$ and $30°$; $\beta = 3.0$ for $\theta = 35°$ and $40°$; $\beta = 3.7$ for $\theta \ge 45°$. As can be seen from Figure 3 and 4, the FEM results match to the results from [12] and

[13] very well. Since around the grating lobe angle, the $(-1,0)$ modes decays slowly along z direction, and then propagates at the grazing angle, the PML cannot absorb the $(-1,0)$ modes very well. Therefore the FEM solution tends to smooth the magnitude of R around the grating lobe angle. It doesn't show the discontinuity of the derivative of lRl at the grating lobe angle.

To further validate the method, we consider the analysis of the plane wave scattering by some periodic structures. Usually in the scattering analysis, the reflection and transmission coefficient are preferred. The computation of the reflection and transmission coefficient can be obtained from the Floquent harmonic expansion. Once the scattered field in a single unit cell is calculated using the FEM, the scattered field just below the upper PML and just above the bottom PML is sampled to derive the reflection and transmission coefficient. The reflected field and transmitted field is a superposition of Floquent harmonics [6]:

$$\begin{aligned}\vec{E}^{ref} &= \sum_{m=-\infty}^{+\infty}\sum_{n=-\infty}^{+\infty}\left[c_{mn}^{ref}\vec{F}_{mn}^{TE} + d_{mn}^{ref}\vec{F}_{mn}^{TM}\right], \\ \vec{E}^{tr} &= \sum_{m=-\infty}^{+\infty}\sum_{n=-\infty}^{+\infty}\left[c_{mn}^{tr}\vec{F}_{mn}^{TE} + d_{mn}^{tr}\vec{F}_{mn}^{TM}\right],\end{aligned} \tag{27}$$

where c_{mn} and d_{mn} are the unknown coefficients, and $\vec{F}_{mn}^{TE}$ and $\vec{F}_{mn}^{TM}$ are the Floquent harmonics,

$$\begin{aligned}\vec{F}_{mn}^{TE} &= \frac{\alpha_n\vec{x} - \alpha_m\vec{y}}{\sqrt{A\left(\alpha_n^2+\alpha_m^2\right)}}e^{-j(\alpha_m x+\alpha_n y)}e^{-j\beta_z z}, \\ \vec{F}_{mn}^{TM} &= \frac{\alpha_m\hat{x} + \alpha_n\hat{y} - \left(\alpha_m^2+\alpha_n^2\right)/\beta_z\hat{z}}{\sqrt{A\left(\alpha_n^2+\alpha_m^2\right)}}e^{-j(\alpha_m x+\alpha_n y)}e^{-j\beta_z z}.\end{aligned} \tag{28}$$

Here

$$\begin{aligned}\alpha_m &= k_0\sin\theta\cos\phi + \frac{2\pi m}{D_x} \qquad & \alpha_n &= k_0\sin\theta\cos\phi + \frac{2\pi n}{D_y} \\ \beta_z &= \sqrt{k_0^2-\alpha_m^2-\alpha_n^2} & A &= D_xD_y\end{aligned} \tag{29}$$

Making use of the orthogonality of Floquent harmonics, we can separate $\vec{E}^{ref}$ and $\vec{E}^{tr}$ into individual modes. From c_{00} and d_{00}, we

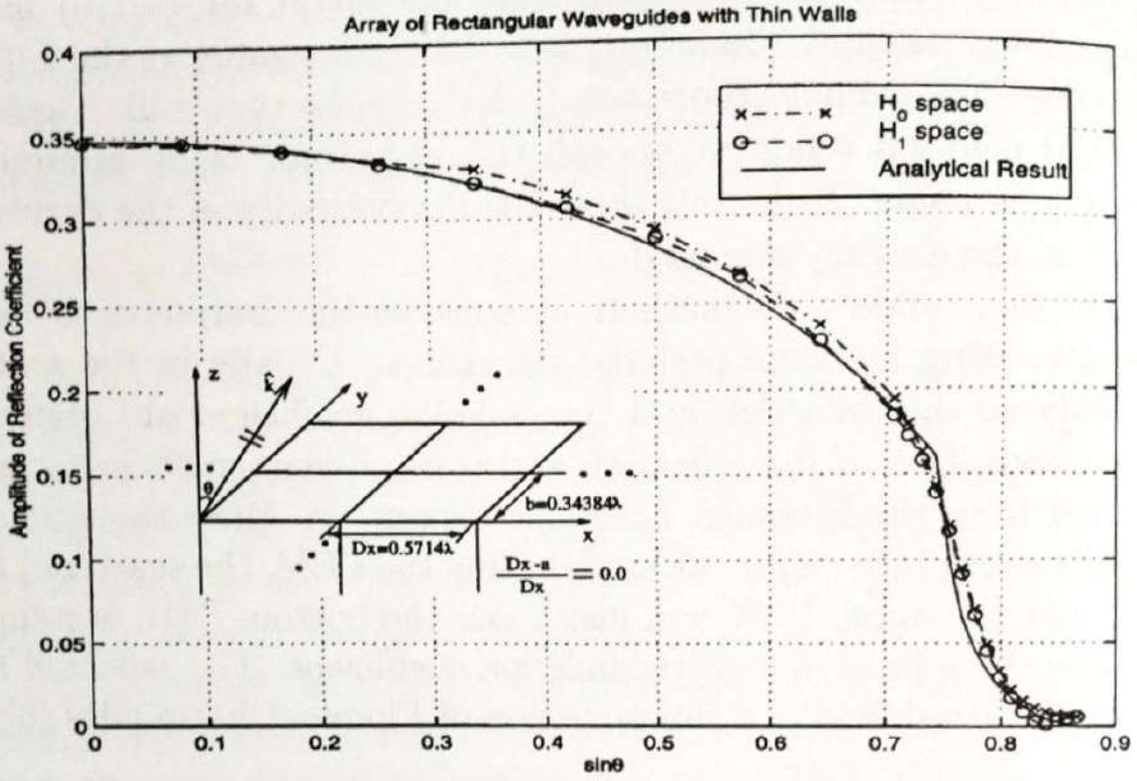

Figure 3. Amplitude of the reflection coefficient for an array of rectangular waveguides with thin walls.

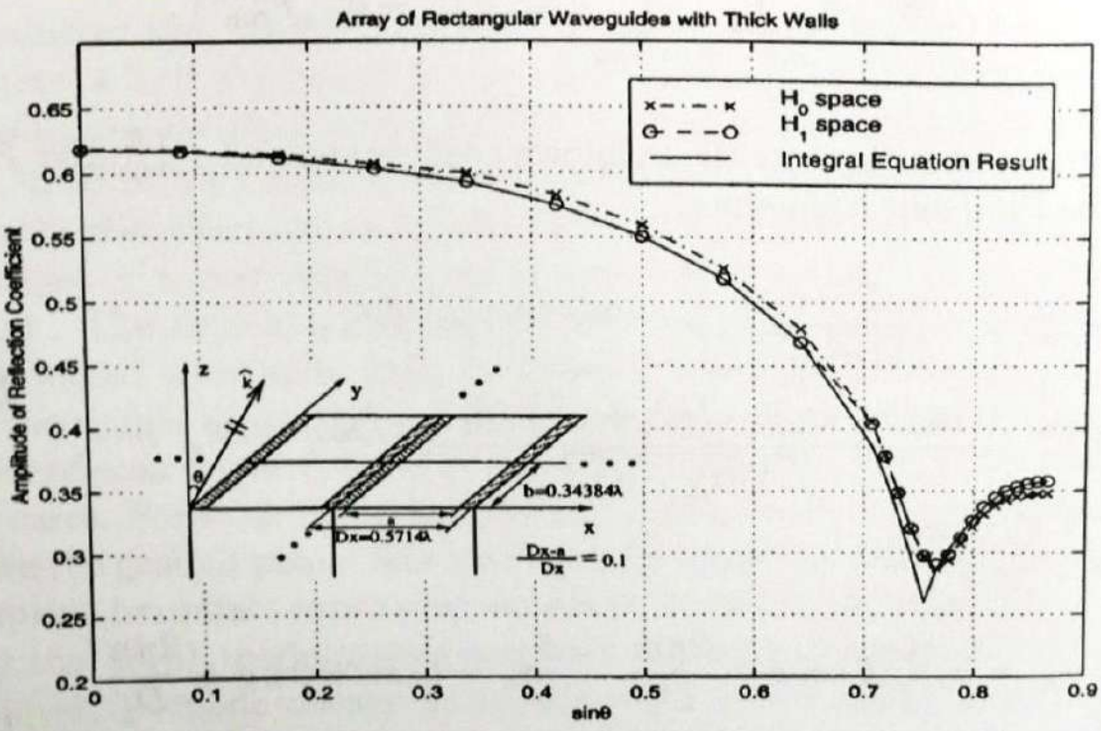

Figure 4. Amplitude of the reflection coefficient for an array of rectangular waveguides with thick walls.

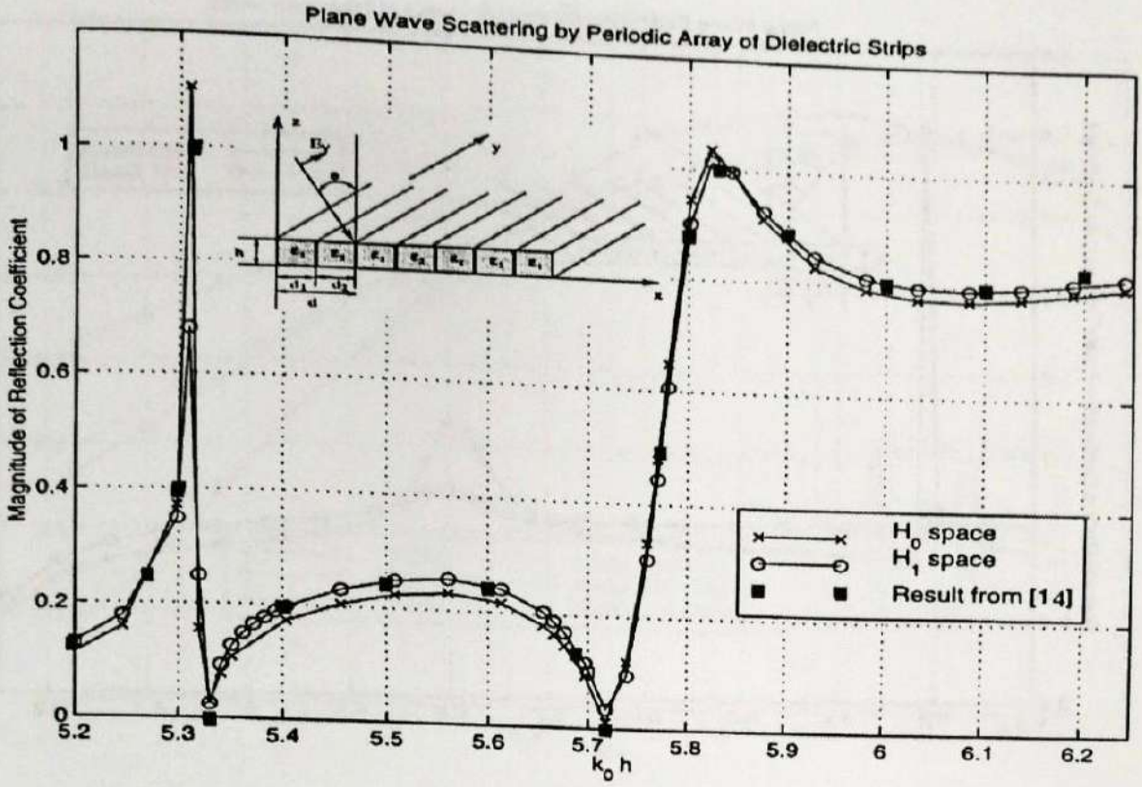

Figure 5. Reflection coefficient for a periodic array of dielectric strips. $\epsilon_1 = 2.56$; $\epsilon_2 = 1.44$. $d_1 = d_2 = d/2$; $h = 1\,\mathrm{m}$; $h/d = 1.713$. The incident plane wave has $\hat{y}$-polarized electric field with $\theta^{inc} = 45°$.

get the reflection and transmission coefficient for the $(0,0)$ Floquent mode.

In the first example of scattering, a dielectric layer with periodically varying dielectric constant is analyzed [14, 15]. The geometry and magnitude of reflection coefficient is shown in Figure 5. The frequency is from 248 to 300 MHz, i.e., $k_0 h$ from 5.2 to 6.28. In the FEM model, the average edge length is 0.05 m. The PML is 0.2 m thick and placed 0.3 m above and below the dielectric slab. $\beta = 3.0$. The FEM results match the results of [14] very well. To further demonstrate the accuracy of the method, Figure 6 shows the summation of power reflection and transmission coefficient. As can be seen, $H_1(curl)$ offers much more accurate result than $H_0(curl)$, especially at the two peaks. When $k_0 h$ approaches 6.3, the error for both $H_0(curl)$ and $H_1(curl)$ increases, due to the slow attenuation of the next Floquent mode, the $(1,0)$ mode.

In the next example, metal meshes with various thickness are analyzed. The size of a single cell in the metal mesh is 1 m ×1 m. The thickness is 0.00 m, 0.10 m, and 0.25. A plane wave is normally incident with the frequency varying from 150 to 300 MHz, i.e., g/λ_0

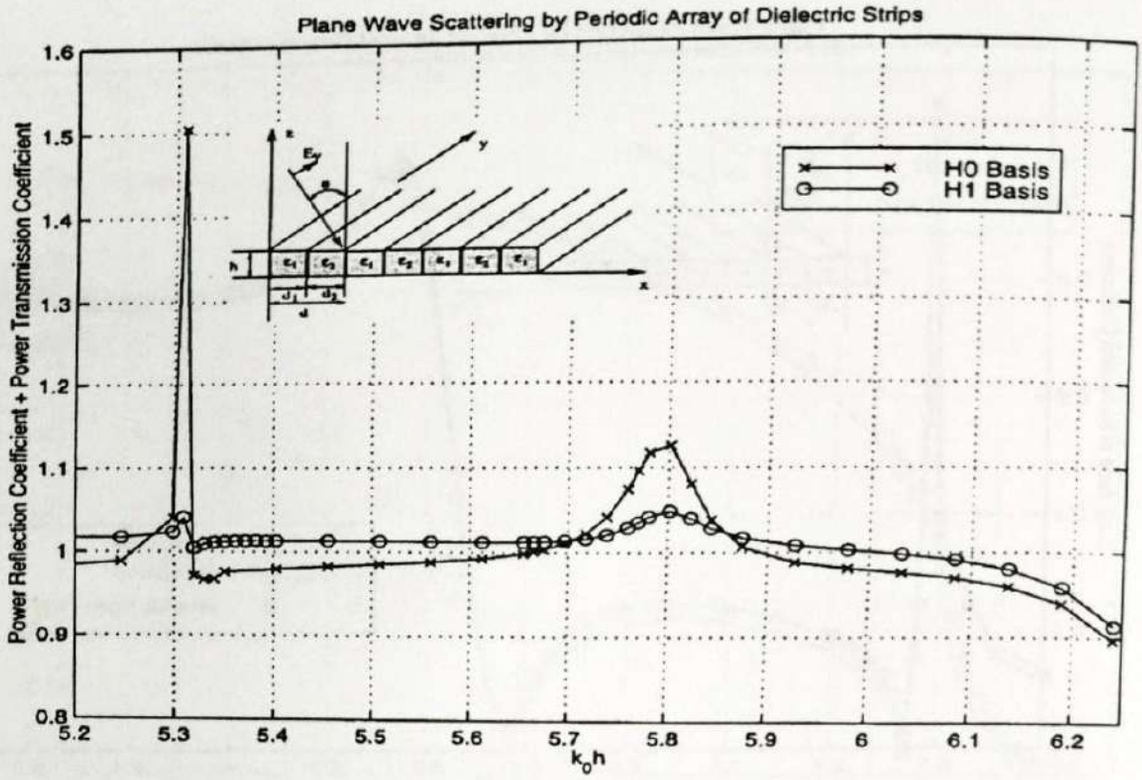

Figure 6. Power reflection coefficient for + power transmission coefficient, $\epsilon_1 = 2.56$; $\epsilon_2 = 1.44$. $d_1 = d_2 = d/2$; $h = 1\,\mathrm{m}$; $h/d = 1.713$. The incident plane wave has $\hat{y}$-polarized electric field with $\theta^{inc} = 45°$.

from 0.5 to 1.0. Since the frequency band is wide, different grids are used to obtain the corresponding segments of the transmittance curve. For $H_0(curl)$ elements, the average edge length is 0.1 m, 0.07 m, and 0.05 m for the g/λ_0 from 0.5 to 0.63, 0.63 to 0.77, and 0.77 to 1.0, respectively. For $H_1(curl)$ elements, the average edge length is 0.1 m and 0.07 m for g/λ_0 from 0.5 to 0.67, and 0.67 to 1.0, respectively. The PML is 4 times the average edge length thick and placed at a distance of 6 times the average edge length from the mesh. The value of β is set to 2.0. Figures 7 and 9 show the transmission curve for $H_0(curl)$ and $H_1(curl)$ elements, respectively. Figures 8 and 10 show the summation of the power reflection and transmission coefficients for $H_0(curl)$ and $H_1(curl)$ elements, respectively. Compared with the results from [16], the results with the $H_1(curl)$ elements match very well, and its summation is very close to one, except when the frequency approaches 300 MHz because the next high order Floquent mode decays very slowly along the z direction at this frequency.

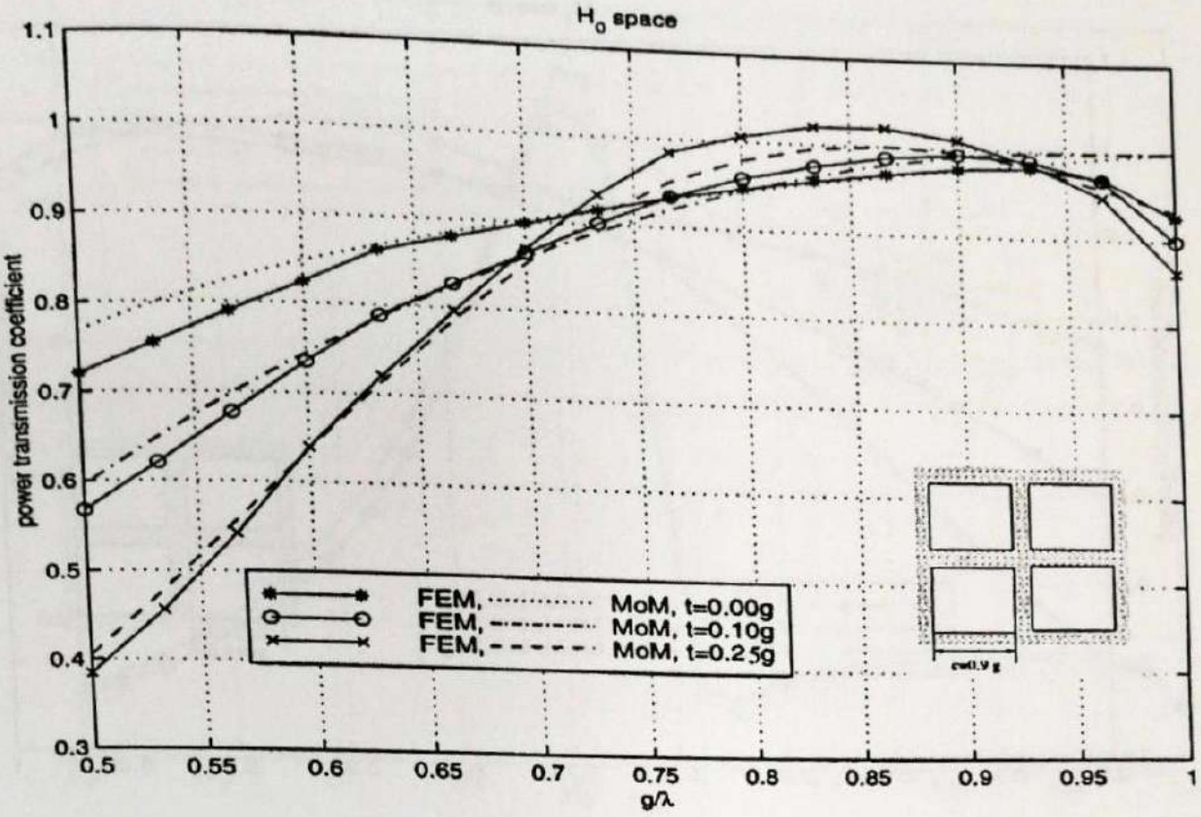

Figure 7. Power transmission coefficient for plane wave normal incidence on a PEC mesh with varying thicknesses. g is period, t is thickness, and c is square hole size. H_0 elements used.

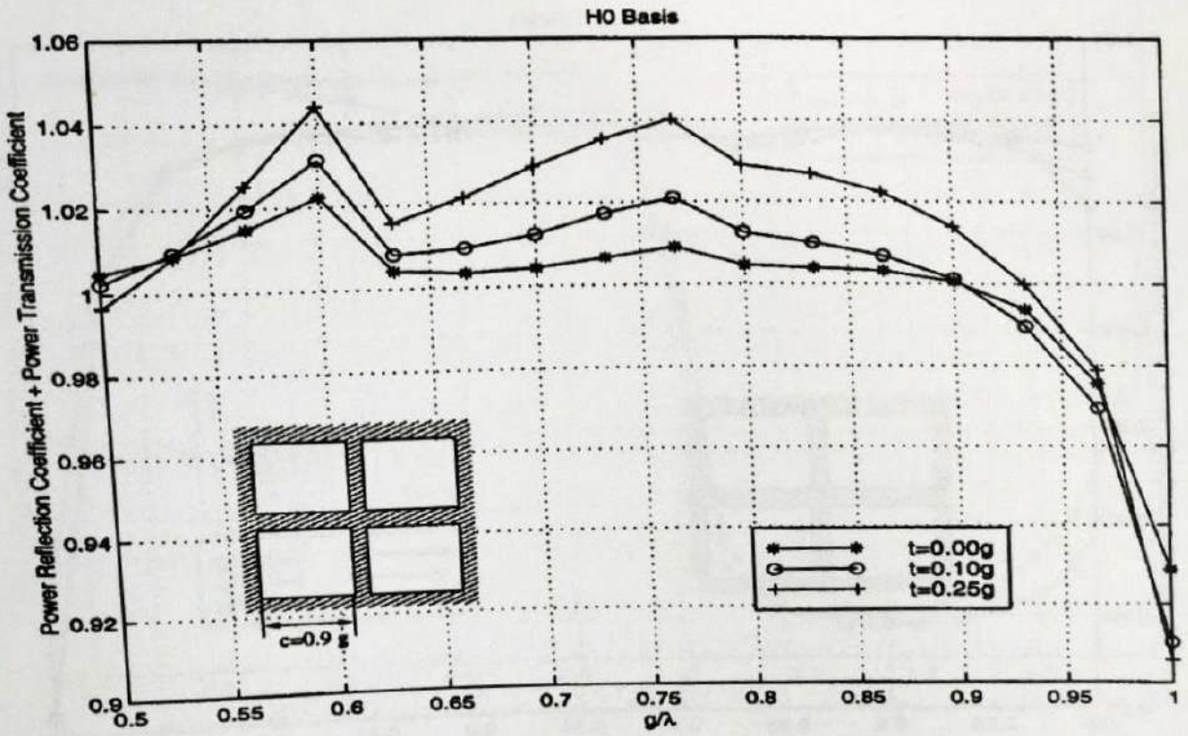

Figure 8. Power reflection coefficient + power transmission coefficient. H_0 elements used.

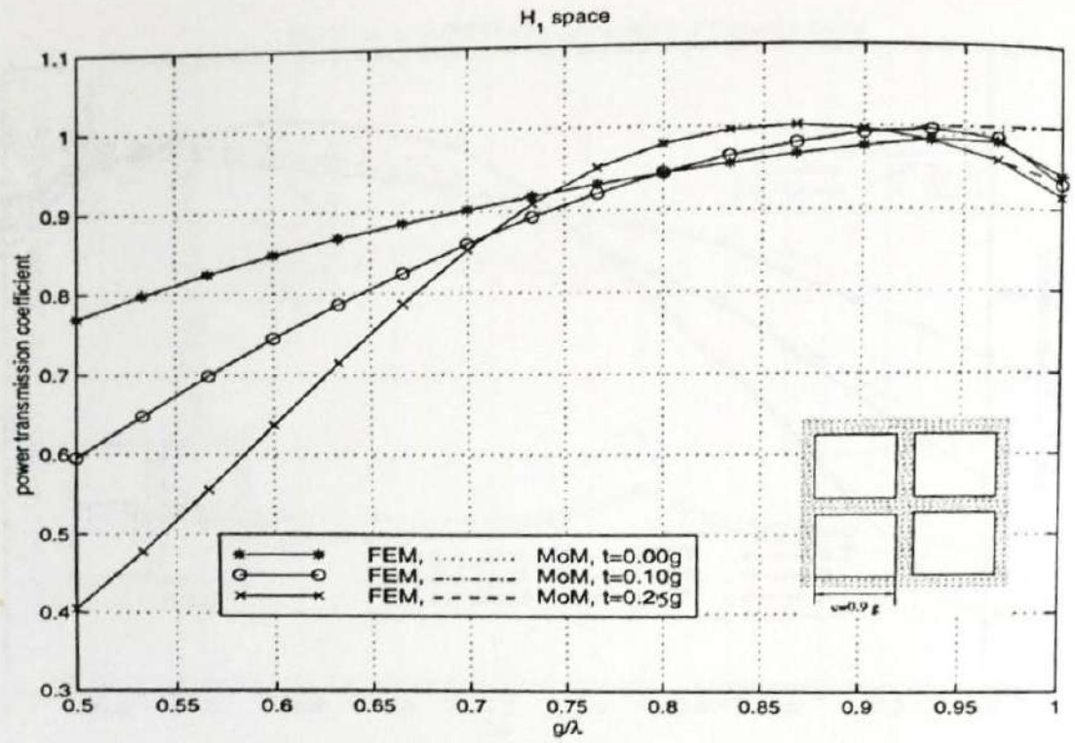

Figure 9. Power transmission coefficient for plane wave normal incidence on a PEC mesh with varying thicknesses. g is period, t is thickness, and c is square hole size. H_1 elements used.

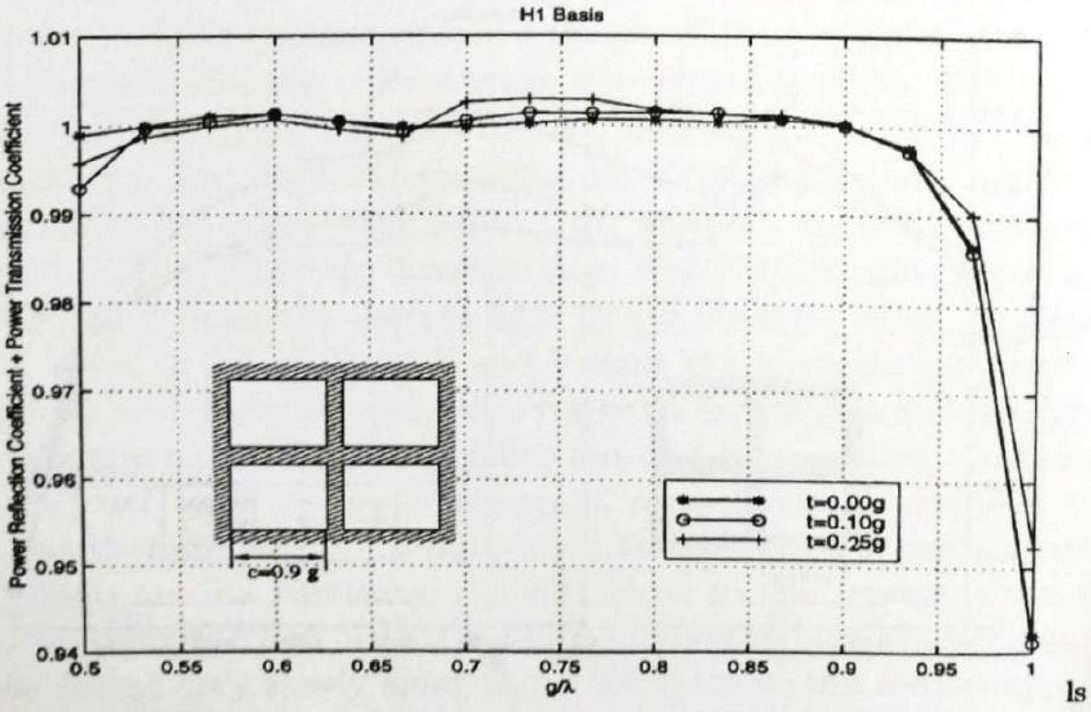

Figure 10. Power reflection coefficient + power transmission coefficient. H_1 elements used.

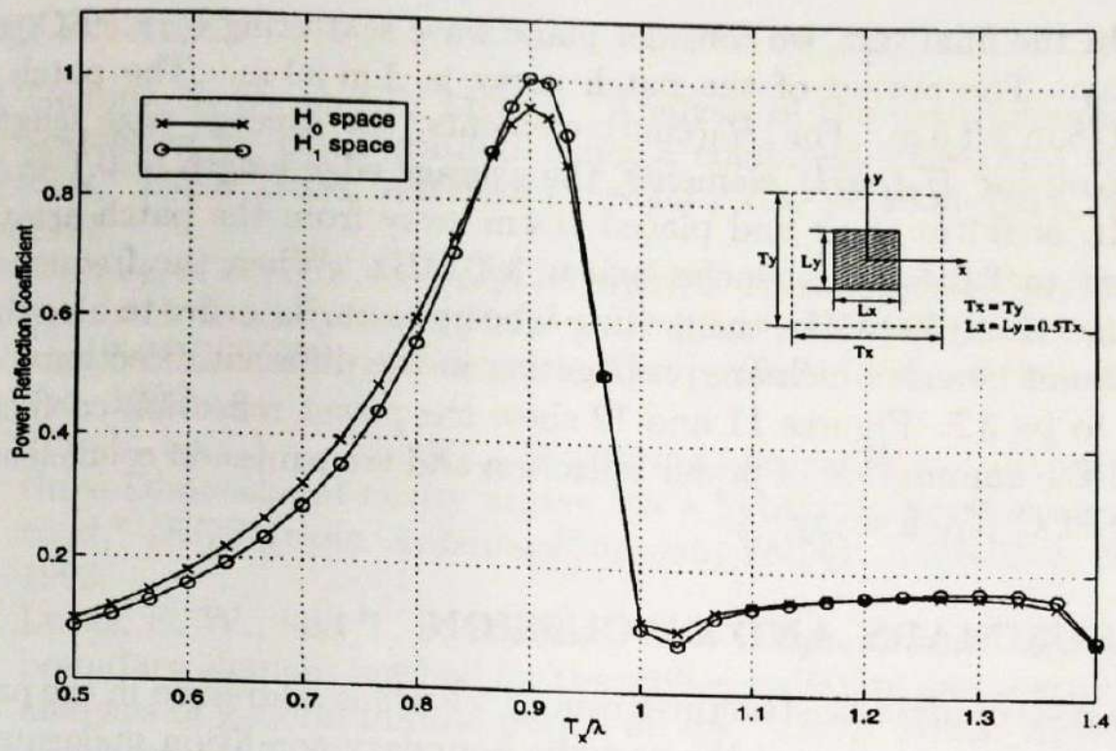

Figure 11. Power reflection coefficient. The incident plane wave has $\hat{y}$-polarized electric field, normal incidence.

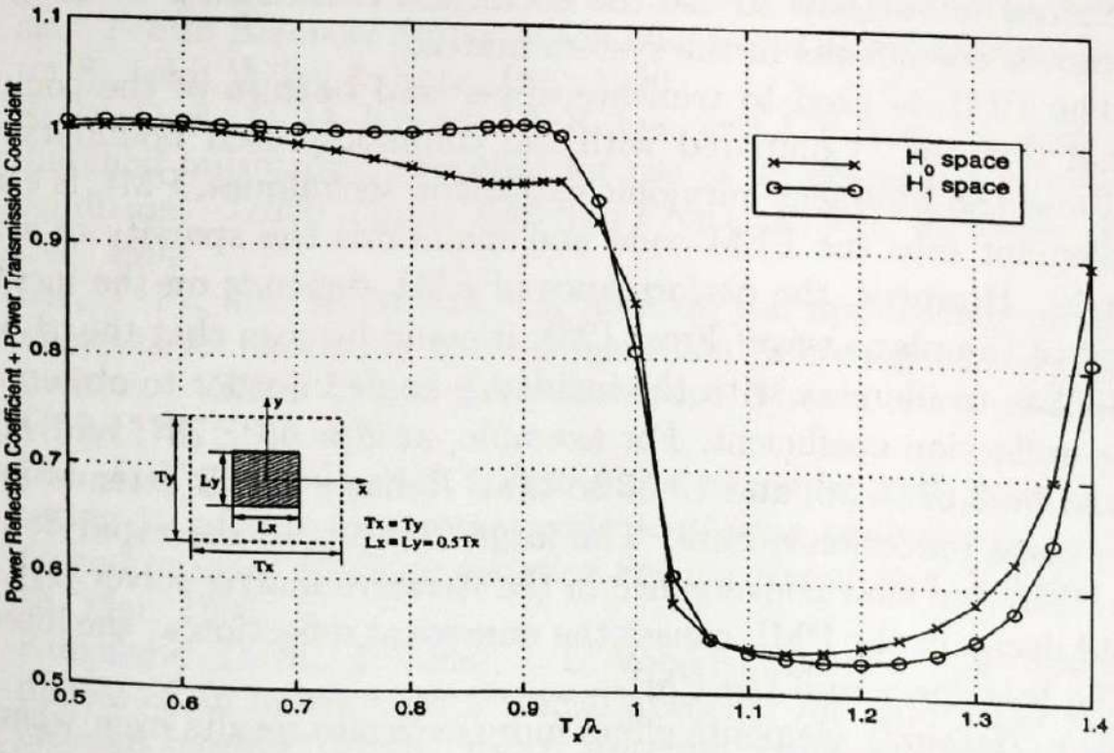

Figure 12. Power reflection coefficient + power transmission coefficient. The incident plane wave has $\hat{y}$-polarized electric field, normal incidence.

In the final test, we consider plane wave scattering by a PEC patch array. The period of the patch array is $1\,\mathrm{m} \times 1\,\mathrm{m}$. The patch size is $0.5\,\mathrm{m} \times 0.5\,\mathrm{m}$. For $H_0(curl)$ elements, the average edge length is $0.05\,\mathrm{m}$; for $H_1(curl)$ elements, the average edge length is $0.1\,\mathrm{m}$. The PML is $0.3\,\mathrm{m}$ thick and placed $0.4\,\mathrm{m}$ away from the patch array. β is set to 2.0 for frequencies below $300\,\mathrm{MHz}$. When the frequency is higher than $300\,\mathrm{MHz}$, the grating lobe appears. In order to absorb the different beams which are propagating in the different directions, β is set to be 3.5. Figures 11 and 12 show the power reflection coefficient, and the summation of power reflection and transmission coefficient for the PEC patch array.

7. SUMMARY AND DISCUSSION

Analysis of periodic structures using TVFEM is addressed in the paper. The implementation of the periodic boundary condition makes use of the basic property of TVFEM. The relationship between $\vec{E}$ and $\vec{H}$ fields on the opposing walls is converted into the relationship between the unknown coefficients on the opposing walls. A detailed formulation is offered about how to use the coefficient relationship to merge the unknown coefficients in the system matrix.

The PML is used to truncate upper and bottom of the computational domain. Compared with the commonly-used boundary integral and the Floquent harmonic expansion techniques, PML is easy to implement into the FEM code and maintains the sparsity of system matrix. However, the performance of PML depends on the incidence angle of the plane wave. From (26), it could be seen that the β of the PML has to increase with the incidence angle in order to obtain a desired reflection coefficient. For example, at $\theta = 60°$, $70°$, and $80°$, β has to be 3.67, 5.36, and 10.55 so that R has $-40\,\mathrm{dB}$ attenuation; at $90°$, total reflection occurs. The large β leads to the rapid decay in the PML and slow convergence in the iterative matrix solver [11]. The rapid decay in the PML causes the numerical reflection at the interface of the free space and the PML.

The $H_1(curl)$ elements offers more accurate results even when the grid for the $H_1(curl)$ elements is much coarser than the grid for $H_0(curl)$ elements. This is can been seen from the previous numerical results. Therefore, H1(curl) elements are recommended.

REFERENCES

1. Gedney, S. D., and R. Mittra, "Analysis of the electromagnetic scattering by thick gratings using a combined FEM/MM solution," *IEEE Trans. Antenna Propagat.*, Vol. 39, 1605–1614, Nov. 1991.
2. Gedney, S. D., J. F. Lee, and R. Mittra, "A combined FEM/MoM approach to analyze the plane wave diffraction by arbitrary gratings," *IEEE Trans. Microwave Theory Tech.*, Vol. 40, 363–370, Feb. 1992.
3. Jin, J., and J. L. Volakis, "Scattering and radiation analysis of three-Dimensional cavity arrays via a hybrid finite-element method," *IEEE Trans. Antenna Propagat.*, Vol. 41, 1580–1585, Nov. 1993.
4. Lucas, E. W., and T. P. Fontana, "A 3-D hybrid finite element/ boundary element method for the unified radiation and scattering analysis of general infinite period arrays," *IEEE Trans. Antenna Propagat.*, Vol. 43, 145–153, Feb. 1995.
5. McGrath, D. T., and V. P. Pyati, "Phased array antenna analysis with the hybrid finite element method," *IEEE Trans. Antenna Propagat.*, Vol. 42, 1625–1630, Dec. 1994.
6. Angelo, J. D., and I. Mayergoyz, "Phased array antenna analysis," *Finite Element Software for Microwave Engineering*, Chapter 8, John Wiley & Sons, Inc., 1996.
7. Sacks, D. S., D. M. Kingsland, R. Lee, and J. F. Lee, "A perfectly matched anisotropic absorber for use as an absorbing boundary condition," *IEEE Trans. Antenna Propagat.*, Vol. 43, 1460–1463, Dec. 1995.
8. Lee, J. F., and R. Mittra, "A note on the application of edge-elements for modeling three-dimensional inhomogeneously-filled cavities," *IEEE Trans. Microwave)ave Theory Tech.*, Vol. 40, 1767-1773, Sept. 1992.
9. Lee, J. F., "Tangential vector finite elements and their application to solving electromagnetic scattering problems," *Applied Computational Electromagnetics Society Newsletter*, Vol. 10, 52-75, Mar. 1995.
10. Kingsland, D. M., J. Gong, J. L. Volakis, and J. F. Lee, "Performance of an anisotropic artificial absorber for truncating finite-element meshes," *IEEE Trans. Antenna Propagat.*, Vol. 44, 975–981, July 1996.
11. Wu, J. Y., D. M. Kingsland, J. F. Lee, and R. Lee, "A comparison of anisotropic PML to berenger's PML and its application to the finite-element method for EM scattering," *IEEE Trans. Antenna Propagat.*, Vol. 45, 40–50, Jan. 1997.

12. Wu, C. P., and V. Galindo, "Properties of a phased array of rectangular waveguides with thin walls," *IEEE Trans. Antenna Propagat.*, Vol. 14, 163–173, Mar. 1966.
13. Galindo, V., and C. P. Wu, "Numerical solutions for an infinite phased array of rectangular waveguides with thick walls," *IEEE Trans. Antenna Propagat.*, Vol. 14, 149–158, Mar. 1966.
14. Bertoni, H. L., L. S. Cheo, and T. Tamir, "Frequency-selective reflection and transmission by a periodic dielectric layer," *IEEE Trans. Antenna Propagat.*, Vol. 37, 78–83, Jan. 1989.
15. Pinello, W. P., R. Lee, and A. C. Cangellaris, "Finite element modeling of electromagnetic wave interactions with periodic dielectric structures," *IEEE Trans. Micro ave Theory Tech.*, Vol. 33, 1083–1088, Oct. 1985.
16. Compton, R. C., and D. B. Rutledge, "Approximation techniques for planar periodic structures," *IEEE Trans. Microwave Theory Tech.*, Vol. 33, 1083–1088, Oct. 1985.